Adsorption (2007) 13: 9–19
DOI 10.1007/s10450-007-9008-6

Experimental investigation of liquid chromatography columns by means of computed tomography

Dirk-Uwe Astrath · Florian Lottes · Duc Thoung Vu · Wolfgang Arlt · Erling H. Stenby

Received: 11 October 2006 / Revised: 11 October 2006 / Accepted: 12 October 2006 / Published online: 7 April 2007

Abstract The efficiency of packed chromatographic columns was investigated experimentally by means of computed tomography (CT) techniques. The measurements were carried out by monitoring tracer fronts in situ inside the chromatographic columns. The experimental results were fitted using the equilibrium dispersive model (EDM) and varying the so called apparent axial dispersion coefficient. The additivity of the first and second central moments was exploited to estimate column efficiency in different regions of the column.

The results showed that the columns under investigation offered a higher column efficiency in the centre compared to the wall region. Furthermore the void fraction in the vicinity of the walls was lower than that in the column core. For this reason the bands were conveyed faster in the central region of the column where the permeability was higher. This result is in good agreement with earlier findings.

Keywords Chromatography · Computed tomography (CT)

1 Introduction

An efficient operation of chromatographic separations is crucial for preparative applications because the process must run economically. To achieve the necessary high efficiencies of the chromatographic columns, the cross sectional velocity profile should closely match the ideal plug profile. Random or structural velocity variations across the chromatographic bed will contribute to the effective band broadening and hence to deterioration of the overall column performance. The peak resolution as well as the obtainable recovery yield decline. To attain uniform velocity distributions as well as hydrodynamic dispersion, the packing density must approach uniformity.

Commonly, the efficiency of chromatographic columns is evaluated by monitoring the column response to a tracer by use of a bulk detector connected in series with the column. The quantities derived from this kind of experiments are gross parameters which stand for the overall column behaviour but fail to represent local contributions to the overall band broadening addressed above. For this reason, experimental techniques which allow for a locally resolved monitoring of band broadening inside a chromatographic column are desired to relate the underlying transport behaviour of the solvent flow to the overall macroscopic column performance.

Computed tomography (CT) scanning is a modern technique descended from medical technology which permits the in situ monitoring of the progressing tracer fronts. It can be used to gain insight into a variety of physical phenomena associated with transport in porous media (Chaouki et al. 1997; Peters et al. 1996; Karacan 2003) and found special attention for the investigation of problems related to the production of reservoir fluids (Peters and Hardham 1990; Mogensen et al. 2001; Schembre and Kovscek 1996).

The objective of this work was an evaluation of the potential of CT to give information about the local concentration profiles and the degree of packing uniformity inside a chromatographic column. This information is relevant as the

D.-U. Astrath (✉) · F. Lottes · W. Arlt
Lehrstuhl für Thermische Verfahrenstechnik, Institut für Chemie- und Bioingenieurwesen, Friedrich-Alexander University Erlangen-Nuremberg, Egerlandstr. 3, 91058 Erlangen, Germany
e-mail: dirk-uwe.astrath@cbi.uni-erlangen.de

D.T. Vu · E.H. Stenby
Engineering Research Center—Phase Equilibria and Separation Processes (IVC-SEP), Department of Chemical Engineering, Building 229, Technical University of Denmark, 2800 Lyngby, Denmark

separation efficiency of chromatographic columns strongly depends on a homogeneous structure of the packing. Evidence that the structure of the packed bed is not necessarily homogeneous can be found in the literature (Guiochon et al. 1997). In the present study, the efficiency of chromatographic columns with inner diameters of 0.026 m and 0.050 m respectively was investigated, respectively. The experimental results were fitted using the so called equilibrium dispersive model of chromatography (Guiochon and Lin 2003). The additivity of the first and second moment was exploited to determine local axial dispersion coefficients.

2 Theoretical background

2.1 Chromatography

2.1.1 Inhomogeneous column packing

The efficiency of chromatographic separations strongly depends on a homogeneous packing of the stationary phase. Theoretical investigations carried out by Yun and Guiochon (1994) and Yun and Guiochon (1996) have shown that velocity variations in a chromatographic column as caused by an inhomogeneous packing have a similar effect as an increased extent of effective axial dispersion. The profiles of the eluting bands are significantly affected and the productivity in preparative applications is impaired.

Experimental evidence that the packing structure in chromatographic columns is not necessarily homogeneous was summarized in a review article by Guiochon et al. (1997). Chromatographic columns that were packed by so called slurry methods offer a rather homogeneous core region surrounded by a denser and less permeable region in the vicinity of the column wall (Baur et al. 1988; Kamiński 1992; Farkas et al. 1994, 1996, 1997; Farkas and Guiochon 1997; Yun and Guiochon 1997; Brandt et al. 1998). The column efficiency of the wall region is significantly lower than that of the core region (Farkas et al. 1994; Farkas and Guiochon 1997).

Nuclear magnetic resonance imaging is another non-invasive measurement technique derived from medical technology which allows for the observation of inhomogeneities in chromatographic columns. The technique was used to investigate mass transfer, flow phenomena, and dispersion effects in packed beds e.g. (Sedermann et al. 1997, 1998; Götz et al. 2002) and chromatographic columns (Tallarek et al. 1996, 1998a, 1998b; Baumeister et al. 1995). Tallarek et al. (1995) used NMR for the observation of chromatographic bands of Gadolinium compounds. Mitchell et al. (1997) addressed the effects of column packing and distribution non-uniformity on the separation quality. They showed that local band variances were generally lower than the corresponding band variances averaged over the column cross section similar to those monitored in an eluent history detector. Harding and Baumann (2001) observed significant column wall effects strongly depending on the local packing density.

According to Heuer et al. (1996), the neglect of non-uniform packing structures in the models commonly used for the simulation of chromatographic separations leads to discrepancies between the model prediction and the experimental findings while scaling up chromatographic columns.

2.1.2 Efficiency of chromatographic separations

Hydrodynamic dispersion effects result in a reduced efficiency of chromatographic columns as the bands of the components to be separated spread on their way through the column (Schulte and Epping 2005). The dispersion is the result of convection as well as molecular diffusion effects. Convective dispersion is due to velocity distributions at the microscopic scale caused by the adhesion at the surface of the adsorbent particles and the statistical backmixing associated with tortuous pathways through a packed bed.

The efficiency of a chromatographic column is determined by the degree of broadening of the band or front that progresses through the column. It is commonly quantified by parameters associated with the variance or second central moment σ^2 of the individual bands.

$$\sigma^2 = \frac{\int_0^\infty c(t) \cdot (t - \mu_1)^2 \, \mathrm{d}t}{\int_0^\infty c(t) \, \mathrm{d}t} \tag{1}$$

The efficiency or plate number N of a chromatographic column is given by

$$N = \frac{(\mu_1)^2}{\sigma^2} \tag{2}$$

where μ_1 is the first moment or mean residence time of the band. Another common term to describe the lumped effects of hydrodynamic dispersion is the equivalent plate height H. It is worth noting that the efficiency as well as the equivalent plate height are not purely column characteristics but depend on the component of interest.

$$H = \frac{L}{N} \tag{3}$$

Several approaches to correlate the equivalent plate height and the interstitial velocity are known. The equations given by Van Deemter (Van Deemter et al. 1956) and Knox (1977) are most commonly used in the field of chromatography.

2.1.3 Equilibrium dispersive model

Generally, mass transfer models of chromatographic separations deal with two independent variables, the time and the

axial coordinate, and two dependent variables, the mobile phase concentration c_i and the stationary phase concentration q_i. The equilibrium-dispersive model is the easiest mass transfer model accounting for non-idealities in chromatography. It is frequently used for the design and optimization of chromatographic separations (Michel et al. 2005). The model is based on the assumption that the stationary and the mobile phase are in permanent local equilibrium throughout the column. All non-idealities, including band-broadening due to mass transfer resistance are lumped into an apparent axial dispersion coefficient $D_{\mathrm{ax}}^{\mathrm{app}}$ (Seidel-Morgenstern 1993).

$$\frac{\partial c}{\partial t} + F \cdot \frac{\partial q^*}{\partial t} + u \cdot \frac{\partial c}{\partial z} = D_{\mathrm{ax}}^{\mathrm{app}} \cdot \frac{\partial^2 c}{\partial z^2} \tag{4}$$

The assumption that the two phases are in equilibrium throughout the column makes the mass balance for the stationary phase superfluous. The stationary phase concentration can be calculated from the mobile phase concentration via the adsorption isotherm being an algebraic equation.

The apparent axial dispersion coefficient is related to the variance of the eluting bands and can be determined from the equivalent plate height.

$$D_{\mathrm{ax}}^{\mathrm{app}} = u \cdot \frac{H}{2} \tag{5}$$

As already mentioned, the apparent axial dispersion coefficient is not constant but a function of the interstitial velocity.

2.2 Computational tomography

The discussion of the principles of computed tomography is restricted to the fundamentals needed for the sake of comprehensibility. A more detailed discussion of computed tomography can be found elsewhere (McCullough and Payne 1977; Kalender 2005).

The measuring principle is based on the ability of X-rays to pass through almost all matter, albeit with some attenuation. The degree of attenuation depends on the local linear attenuation coefficients as well as on the length of the path and is given by Lambert-Beer's law. The local linear attenuation coefficient is a characteristic property of the particular material. It should be mentioned that Eq. 6 is a simplification as it is based on the supposition that the X-ray beams are monochromatic whereas most beams are polychromatic (Mogensen et al. 2001).

$$\ln\left(\frac{I}{I_0}\right) = \int_0^{S_{\mathrm{Obj}}} -\mu \cdot \mathrm{d}x \tag{6}$$

The intensity of the attenuated beams passing the object is monitored to obtain a projection of the object. From the projection data an image file that consists of an array of CT numbers covering a specified range can be reconstructed using mathematical algorithms. The CT-number is defined as a dimensionless attenuation coefficient in terms of SI-Units.

$$\mathrm{CT} = \frac{\mu - \mu_{\mathrm{H_2O}}}{\mu_{\mathrm{H_2O}}} \cdot 1000 \tag{7}$$

For a porous object like the packing in a chromatographic column, the CT-number is given as the weighted mean of the CT-number of the two phases. In particular the weighted mean of the CT-numbers of the mobile Phase *MP* and the stationary phase *SP* (Kantzas 1994).

$$\mathrm{CT} = \varepsilon \cdot \mathrm{CT}_{MP} + [(1-\varepsilon) \cdot \mathrm{CT}_{SP}] \tag{8}$$

During a breakthrough experiment the column is initially saturated with a mobile phase of known composition (*MP*1). Subsequently the initial mobile phase is displaced by a second mobile phase (*MP*2) having a distinct composition. During the duration of the breakthrough the CT-number depends on the mobile phase saturation *S* and is given by (Peters and Hardham 1990).

$$\mathrm{CT}(t) = \varepsilon \cdot [S_{MP1} \cdot \mathrm{CT}_{MP1} + S_{MP2} \cdot \mathrm{CT}_{MP2}] + [(1-\varepsilon) \cdot \mathrm{CT}_{SP}] \tag{9}$$

The mobile phase saturation *S* is given by the volume fraction of the corresponding mobile phase. Consequently the local saturations *S* during a breakthrough can be determined from three CT images representing each of the saturated states and the breakthrough. Furthermore, it is necessary that the CT-numbers of the pure mobile phases *MP*1 and *MP*2 are known and that their attenuation coefficients are sufficiently different.

3 Experimental

3.1 Set-up

The set-up of the high pressure gradient chromatography system is sketched in Fig. 1. A double piston HPLC pump (K-120, Knauer, Germany) delivered the Methanol (MeOH)/Potassium Iodide solutions (*MP*2) at a flow rate of

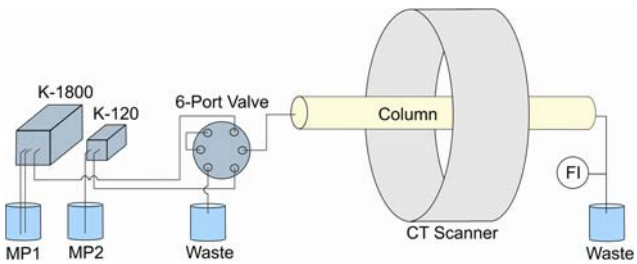

Fig. 1 Experimental set-up

Table 1 Column characteristics

Column #	Inner diameter (mm)	Packing length (mm)
ID 26	26	240
ID 50	50	350

Table 2 Particle size distribution of the ODS material

Diameter	Value (µm)
$d_{1,0}$	49.7
$d_{2,0}$	51.0
$d_{3,0}$	51.7
$d_{1,2}$	53.2

10 ml/min. Another double headed HPLC pump with pulsation suppression (K-1800, Knauer, Germany) conveyed pure methanol (*MP*1) for re-flushing the columns at higher flow rates. A six port valve (Valco) allowed for the mobile phase transition. The valve was placed shortly before the column inlet to reduce extra column band broadening to a minimum. The column, exposed to ambient temperature, was mounted on the patient table of a CT scanner which allowed the column to be moved along its axis during the experiments.

During each of the frontal analysis experiments, the breakthrough behaviour of the progressing front was monitored in four column cross sections at reduced axial positions $z^* = z/L$ of $z_1^* = 0.05$, $z_2^* = 0.35$, $z_3^* = 0.65$, and $z_4^* = 0.95$, respectively. Scans of each cross section were taken until the front had passed before moving the column to the next monitoring position. The maximum acquisition frequency was approximately 0.2 Hz. After each breakthrough experiment, the column was equilibrated for at least two column volumes before the images of the saturated state were taken at all monitoring positions. A flow meter was located behind the column to observe the flow stability of the pumps. The volumetric flow rates where found to be accurate within 2% of the indicated values for all experiments.

3.1.1 CT-scanner

A fourth generation CT-scanner (Siemens Somatom plus) was used for all experiments. The settings for data acquisition of the CT scanner were as follows: slice thickness 2 mm, scan time 2 s, energy parameters 137 kW and 255 mA.

3.1.2 Columns

Two static axial compression columns made of glass (Goetec Labortechnik, Germany) with different inner diameters were investigated experimentally. The distribution system of the columns consisted of a combination of a sintered glass plate and a tissue filter for holding back the stationary phase material.

Steel columns could not be used as steel causes artefacts in the CT images. The columns were packed with a polydisperse, hydrophobic octadecyl stationary phase (ODS) based on a silica gel matrix (C-Gel 560 C18 40–63 µm, Zeochem AG, Switzerland). The particle size distribution and the Sauter mean diameter of the stationary phase material were determined by photoelectric sedimentation analysis.

A non-polar, reversed phase system was used to reduce interactions between the ionic tracer and the stationary phase to a minimum. Both columns were slurry packed with isopropanol as the pushing solvent. Isopropanol was filtered and degassed before use. The compression pressure during the packing operation was 10 bar. This was close to the maximum operating pressure of the large diameter column.

3.1.3 Mobile phases

Methanol (*MP*1) and solutions of potassium iodide (KI) in methanol (*MP*2) were used as mobile phases. The concentrations of the solutions were 20 g/l (2%) and 40 g/l (4%), respectively. Potassium iodide was chosen due to the high atomic mass of iodine which allows for a good contrast in the CT images.

The dependencies of the CT numbers on the mobile phase concentration of potassium Iodide were determined for the packed chromatographic columns. In either column they exhibited a linear relationship against the tracer salt concentration so permitting the use of Eq. 9 for the interpretation of the CT images.

4 Results and discussion

4.1 Band profiles and intra column breakthrough curves

Representative images of the intra column "breakthrough" behaviour are shown in Fig. 2. It can be observed that the intra column concentration profile is not evenly distributed over the column cross. The concentration step is firstly visible near the middle of the cross section. At the margins the concentration change lags behind. Similar band shapes were found e.g. by Brandt et al. (1998). According to Brandt, this warped, parabolic shape of the band is at least partly due to a non-optimal design of the inlet distribution system. Transporting the tracer to the wall region of the glass columns takes additional time. Thus the concentration front close to the wall falls behind during the distribution process. This contributes to the concave shape of the migrating band. It should be emphasized that the molecules in the centre of the

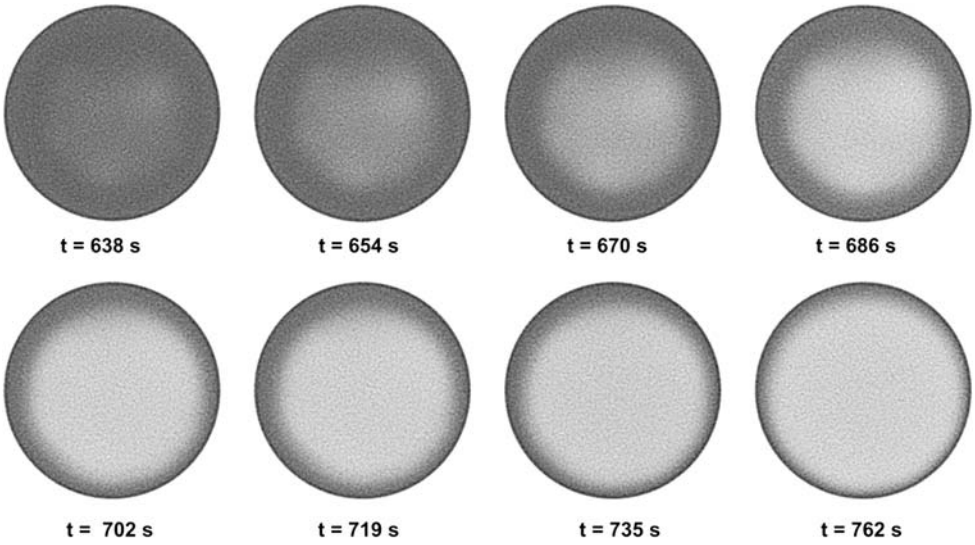

Fig. 2 Successive breakthrough of a KI/MeOH-solution (4%) replacing MeOH in the ID 50 column at $z^* = 0.35$. *White regions* refer to KI/MeOH-solution; *dark regions* refer to pure MeOH. The superficial velocity is 8.5×10^{-5} m/s

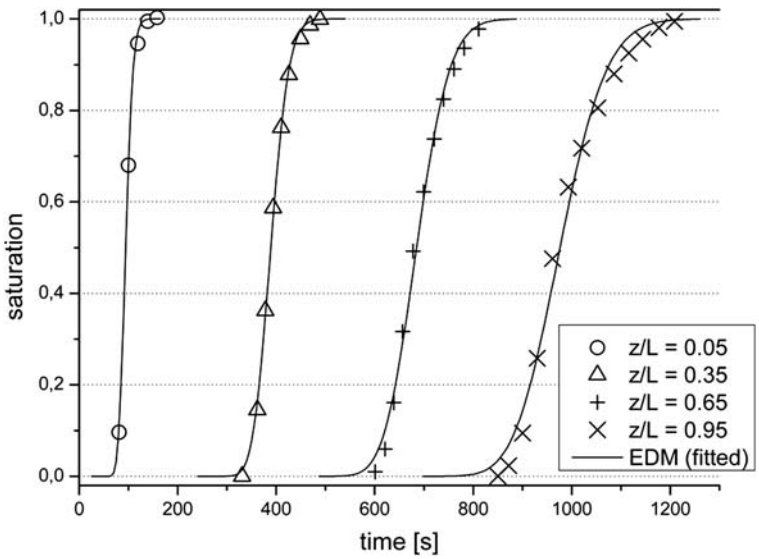

Fig. 3 Experimental and simulated (EDM) intra column saturation fronts for the ID 26 column at different axial positions. KI/MeOH-solution (2%) replaces pure MeOH. The superficial velocity is 31.4×10^{-5} m/s

column elute in the front part of a band or a peak (in case of pulse injection). Those molecules eluting from the larger region close to the column wall lag behind in the rear part or tail and represent a major proportion of the substance. As a consequence the band or peak exhibits tailing if recorded with a bulk detector at the column outlet.

Based on Eq. 9, the intra column breakthrough curves of the salt solutions were determined. For this purpose, the CT images were firstly processed using the public image processing program ImageJ. The image sections showing the packed cross section of the column were extracted. The extracted data were then saved as an array consisting of x- and y-coordinates as well as CT-numbers. MATLAB was used for further data processing and the calculation of the saturations.

Results for the 26 mm as well as the 50 mm column are given in Figs. 3 and 4, respectively. As expected, the tracer bands spread continuously while progressing through the columns giving rise to a monotonic increase of the variance σ^2 of the bands.

The parameters of the equilibrium dispersive model (EDM) were fitted to the experimental data. For non-adsorbing components, an analytical solution of the EDM exists as a function of two parameters, the Peclet number Pe_z and the dimensionless time τ, only (Guiochon and Lin 2003).

$$S = 0.5 + 0.5 \cdot \mathrm{erf}\left[\frac{\sqrt{Pe_z}}{2}(\sqrt{\tau} - \sqrt{1/\tau})\right] + 0.5 \cdot \exp(Pe_z) \cdot \mathrm{erfc}\left[\frac{\sqrt{Pe_z}}{2}(\sqrt{\tau} + \sqrt{1/\tau})\right] \quad (10)$$

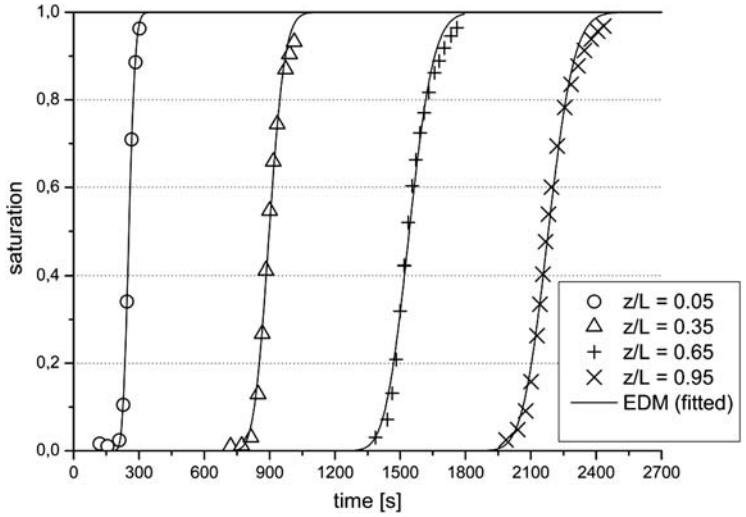

Fig. 4 Experimental and simulated (EDM) intra column saturation fronts for the ID 50 column at different axial positions. KI/MeOH-solution (4%) replaces pure MeOH. The superficial velocity is 8.5×10^{-5} m/s

Table 3 Parameters of the EDM. Parameters are fitted to the intra column breakthrough curves shown in Figs. 3 and 4

Position	ID 26		ID 50	
	t_z^R (s)	Pe_z	t_z^R (s)	Pe_z
$z_1^* = 0.05$	95	131	255	252
$z_1^* = 0.35$	390	365	900	518
$z_1^* = 0.65$	687	337	1544	614
$z_1^* = 0.95$	979	345	2180	1082

$$Pe_z = \frac{u \cdot z}{D_{\text{ax}}^{\text{app}}} \tag{11}$$

$$\tau = \frac{t}{t_z^R} \tag{12}$$

Representative matched curves are shown together with the experimental data in Figs. 3 and 4, respectively. The parameters are given in Table 3. It must be emphasized that the Peclet numbers Pe_z at the different axial positions cannot be compared directly for the reason that they depend linearly on the axial position z.

The fitted curves represent the experimental curves rather well with the exception of the very beginning and the end of each graph. In these regions deviations from the experimental curves were found at some axial positions. As explained above, this phenomenon is likely to be due to radial non-uniformities of the column packing.

Anyway, the low Peclet numbers given in Table 3 indicate low efficiencies of the investigated columns. This is mainly due to the maldistribution caused by the simple distribution systems. The quality of the packed beds was determined independently of the performance of the inlet and outlet frits between the first and the last monitoring position. They exhibit a moderate efficiency. The parameters correlated with the efficiency of the columns are given in Table 4. The fact

Table 4 Reduced HETP and dispersion coefficients of the ID 26 and ID 50 columns. Parameters refer to the zone $z* = 0.05 \ldots 0.95$. Parameters were calculated from the band variances derived from the fitted EDM curves

Column #	ID 26	ID 50
$h = H/d_{1,0}$ (–)	15	7
$D_{\text{ax}}^{\text{app}}$ (m^2/s) $\times 10^{-8}$	9.15	2.88

that the columns are of moderate efficiency only is believed to be due to the relatively low packing pressure caused by the use of glass columns.

In order to investigate the homogeneity and the radial dependency of the column properties in more detail, each of the three column segments enclosed by the monitoring positions was subdivided into ten annuli of equal width (with respect to the columns radius). Contrary to other studies of flow behaviour in packed beds (Sedermann et al. 1997, 1998; Götz et al. 2002), the voids between the particles were not resolved due to the small particle size and the extremely high aspect ratios of the column to particle diameter.

The EDM was then fitted to the breakthrough curves corresponding to each of the annulus segments. The results for the inner (core region) and outer annulus (wall region) are given in Figs. 5 and 6. It is evident that the bands travel faster in the central region than in the vicinity of the column wall. Accordingly the mobile phase preferentially percolates through the core region of the column where the permeability is higher. The increased permeability which gives rise to higher linear velocities is reflected in shorter residence times in the interior of the chromatographic columns. The observation that the packing exhibits different properties in the core and the vicinity column of the column is commonly referred to as the column wall effect (Brandt et al. 1998). Its likely cause is friction of the packing against the column wall (Guiochon et al. 1997).

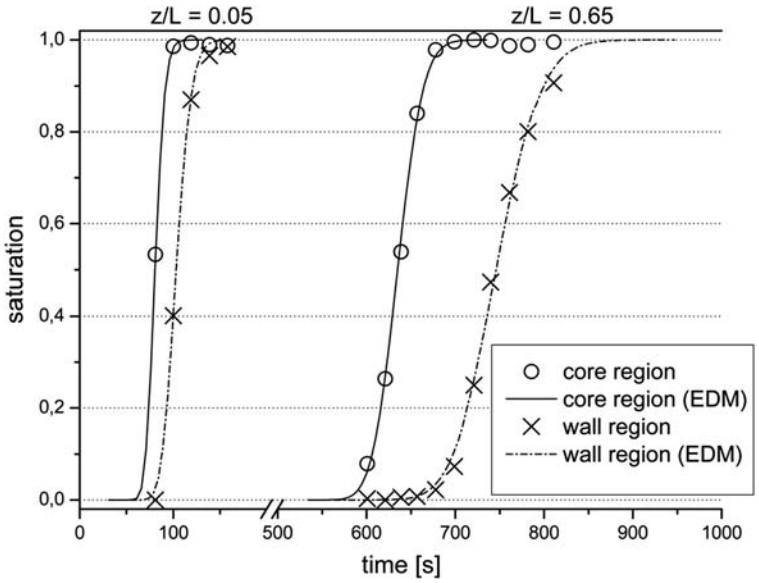

Fig. 5 Comparison of the saturation fronts in the core and the wall region of the column at different axial positions of the ID 26 column. KI/MeOH-solution (2%) replaces pure MeOH

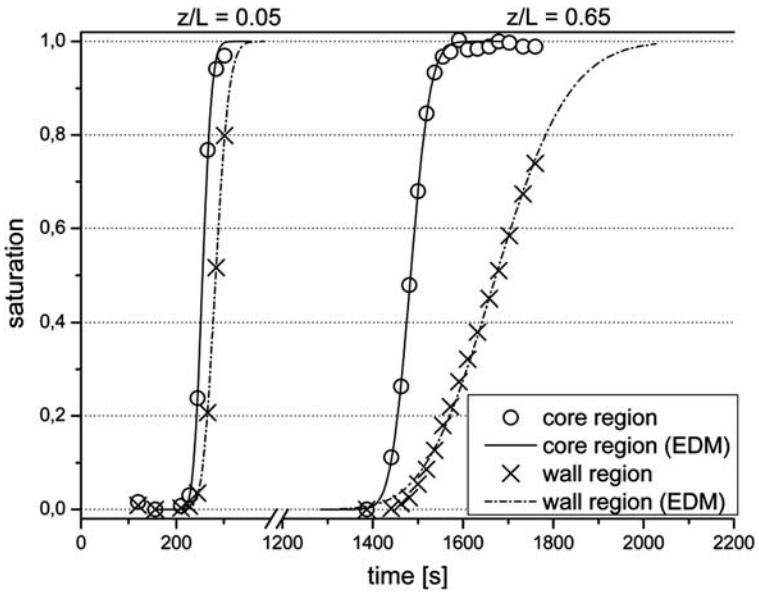

Fig. 6 Comparison of the saturation fronts in the core and the wall region of the column at different axial positions of the ID 50 column. KI/MeOH-solution (4%) replaces pure MeOH

Moreover, the concentration profiles close to the column wall have much stronger spread than the corresponding profiles in the inner annulus. The effect is particularly pronounced in the ID 50 column. The observation that the dispersion phenomena are more influential and that the tracer bands spread more strongly in the wall region is in good agreement with earlier findings by Östergren and Trägårdh (2000) who investigated the hydrodynamic dispersion effects of chromatographic columns packed with beads made of glass and Sephadex G-75, respectively, by mounting concentric electrodes into the columns.

The dependency of the local column properties was investigated more closely by making use of the additivity of the retention time and the variance of the tracer bands.

4.2 Linear velocities

The additivity of the first moment was used to determine linear tracer velocities v_{KI} as a function of the column radius for the single column sections.

$$v_{KI}(r, \Delta z) = \frac{z_{i+1} - z_i}{t_R^F(r, z_{i+1}) - t_R^F(r, z_i)}, \quad i = 1..3 \tag{13}$$

The results of the analysis are shown in Figs. 7 and 8. The core velocities used to normalize the data are given in Table 5. With the exception of the last zone in the ID 50 column all zones exhibit the same, typical dependency of the axial linear velocity on the radial position inside the column. The velocity profile is rather homogeneous in the central region of the column. With increasing radius the linear velocities

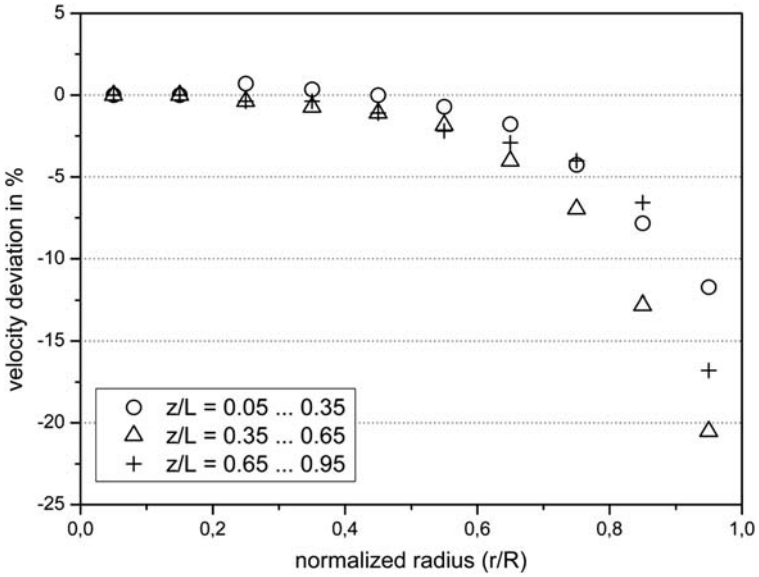

Fig. 7 Radial linear velocity profiles of the potassium iodide bands in different axial zones of the ID 26 column. Velocity deviations are given with respect to the core velocity (inner annulus) of the column. Core velocities are given in Table 5

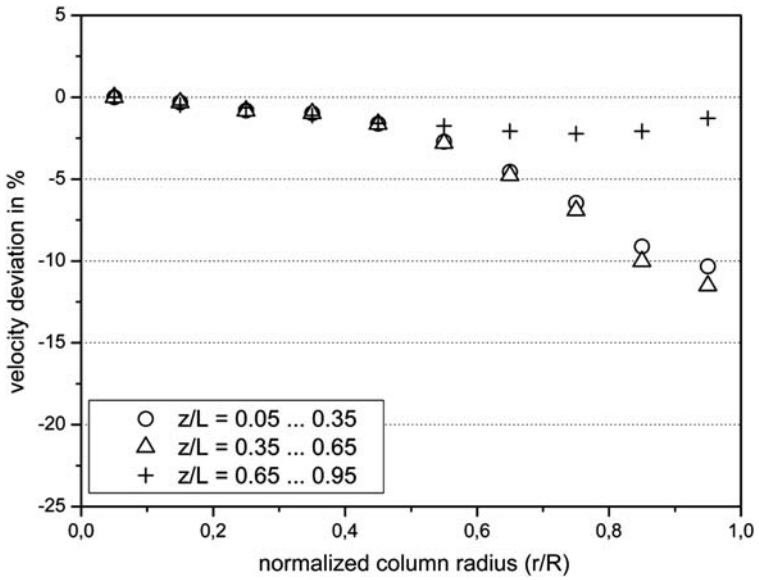

Fig. 8 Radial linear velocity profiles of the potassium iodide bands in different axial zones of the ID 50 column. Velocity deviations are shown with respect to the core velocity (inner annulus) of the column. Core velocities are given in Table 5

decrease monotonically and reach their minimum next to the wall. The velocity deviation is up to 20% in the ID 26 column. The less homogeneous velocity distribution of the smaller column also explains the lower efficiency in terms of the reduced plate height h as given in Table 4.

The velocity profiles are somewhat different from findings reported for randomly packed beds of uniformly sized beads and gas phase systems. Here the wall effect results in increased flow velocities close to the wall (Sedermann et al. 1997) because of a more ordered packing with higher porosities. This is likely to be due to the lack of compression stresses associated with the packing of chromatographic columns.

Similar results concerning the shape of the velocity and corresponding concentration profiles reported here were found in several previous investigations of chromatographic columns, e.g. (Farkas et al. 1994, 1996, 1997). Commonly the mobile phase velocity in the column core is 2 to 8% higher (Guiochon et al. 1997). Yun et al. (Yun and Guiochon

Table 5 Core velocities for different axial zones. Core velocities are calculated based on the intra column retention times of the respective annulus segments

Zone	u_{KI} (core) (m/s)	
	ID 26	ID 50
$z_1^* = 0.05 \ldots 0.35$	0.000256	0.000173
$z_1^* = 0.35 \ldots 0.65$	0.000264	0.000167
$z_1^* = 0.65 \ldots 0.95$	0.000263	0.000173

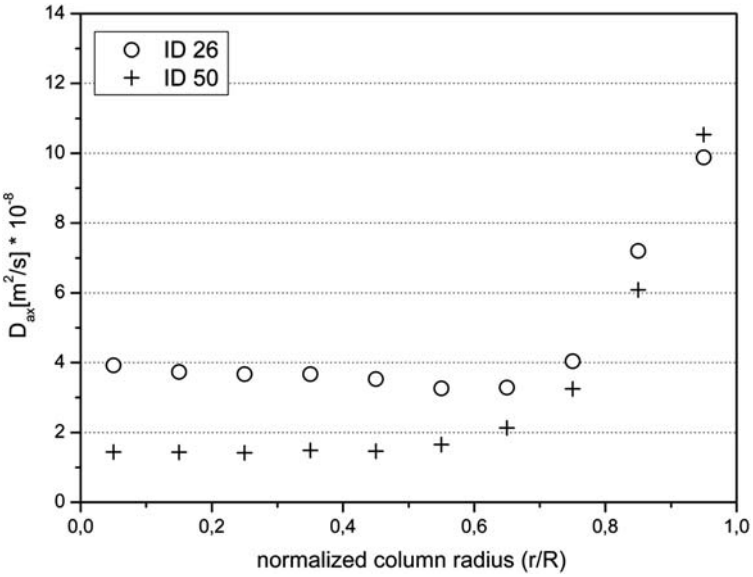

Fig. 9 Radial dispersion variation across the ID 26 and the ID 50 column. The dispersion measurements were carried out between the first and the last monitoring position

1997) found velocity deviations as high as 13% by investigating the radial distribution of an immobilized dye band after removing the packing from the column and cutting it into two halves. The dye was injected into an axial compression column skid having similar dimensions as the columns used in the present study. As already mentioned, the relatively high velocity deviations found in this work are believed to be due to the low packing pressure. Applying higher packing or dynamic compression pressures should result in more homogeneous though still non-uniform distribution of the column external porosity and permeability.

4.3 Column efficiency

The additivity of the variance was used to determine dispersion coefficients for the annulus segments in between the first and the last monitoring position (Lode et al. 1998).

$$\sigma^2(r, z_4) = \sigma^2(r, z_1) + \sigma^2(r, \Delta z_{1\ldots4}) \tag{14}$$

The variances as well as the retention times of the intra column breakthrough curves were obtained from the fitted EDM curves. Subsequently the apparent axial dispersion coefficient of the sections of interest was calculated using Eqs. 2, 3, and 5, respectively.

$$D_{\mathrm{ax}}^{\mathrm{app}} = \frac{1}{2} \cdot \frac{\sigma^2(r, \Delta z_{1\ldots4})}{(t_R^F(r, z_4) - t_R^F(r, z_1))^2} \times \frac{(z_4 - z_1)^2}{t_R^F(r, z_4) - t_R^F(r, z_1)} \tag{15}$$

As can be seen in Fig. 9, the dispersive effects are more pronounced in the region next to the column wall in both columns. Whereas the trend of the dispersion coefficient is rather flat in the central region of the column, it rises significantly towards the column wall. The homogeneous, central region in both columns expands to approximately 65% of the column diameter which is in excellent accordance with findings from Farkas et al. (1997) who report that in larger scale columns the central core region has a diameter on the order of two-thirds of the column diameter. For the more efficient ID 50 column, the dispersion coefficient next to the column wall is approximately five times higher compared to the column core. For the less efficient ID 26 column, the efficiency of the core is generally lower. In the wall region both columns have equivalent efficiencies. It is worth noting that the dispersion coefficients recorded for the single annulus sections is generally lower than the overall dispersion parameters given in Table 4. Only the value of the parameter measured in the direct vicinity of the ID 50 column is close to the value of the gross parameter. This is due to the wide velocity distributions causing the molecules in the central region to precede. Because of this distortion the apparent total band width in the axial direction is larger than the local bandwidth.

The observation is in good agreement with conclusions from (Baumeister et al. 1995; Tallarek et al. 1995; Mitchell et al. 1997) where the homogeneity of column packings was invastigated by means of NMR techniques. The experimental findings obtained by NMR are not superimposed by cross sectional maldistributions or distribution problems but represent local column efficiencies. The results confirmed that local separation efficiencies are frequently better than the effective efficiencies measured by means of a bulk detector at the column outlet. This underlines the impact of velocity and concentration distribution on the column efficiency. The performance of a column with a locally high efficiency can deteriorate seriously in the presence of a maldistributed ve-

locity profile. The greater differences in the retention times of the core region (peak front) and wall region (peak tail) are reflected by broader peaks and reduced efficiencies. Similar trends for the dependency of the dispersion coefficient on the radial coordinate in medium diameter columns were published by Östergren and Trägårdh (2000) who found that the dispersion coefficient rises with increasing column radius. The dispersion coefficient next to the column wall was two to four times higher next to the wall than in the column centre. Less distinct results were recorded by Farkas et al. (1997) using a 50 mm ID axial compression column skid. The efficiency in the wall region was found to be approximately 25% lower compared to the column core.

5 Conclusions

X-ray computed tomography was used to observe the breakthrough behaviour and efficiencies of chromatographic columns made of glass in situ. The measurement technique proved itself to be a well suited tool for the non-invasive characterisation of columns which are opaque for x-rays. The intra column breakthrough behaviour as well as local column properties could be observed without the necessity to install elaborate detection devices inside or at the exit of the column. Although the results based on a limited number of investigated columns must be interpreted with caution, evidence was found that the properties of the packing are not evenly distributed within the column. The packed beds under investigation offered a denser and less efficient wall region compared to the column core. This is in good agreement with earlier findings (Guiochon et al. 1997) providing additional evidence that the porous bed in slurry packed columns is heterogeneous in the radial direction.

List of symbols

c	concentration
CT	CT number
$D_{\mathrm{ax}}^{\mathrm{app}}$	apparent axial dispersion coefficient
d	particle diameter
ε	porosity
F	phase ratio
H	height equivalent to a theoretical plate
h	reduced plate height
I	radiation intensity
L	column length
L^{sample}	length of sample investigated by CT
μ	attenuation coefficient
μ_1	first moment of a band/peak
N	number of theoretical plates
Pe_z	Peclet number at position z
R	column radius
r	radial coordinate
S	mobile phase saturation
σ^2	variance of the band
t	time
t_z^R	retention time of front at position z
τ	dimensionless time
u	linear velocity
z	axial coordinate
z^*	reduced axial coordinate

Acknowledgements The authors want to thank the Technische Universität Berlin where parts of this work were conducted. Furthermore they want to express their gratitude to Zeochem AG for kindly providing the stationary phase material.

References

Baumeister, E., Klose, U., Albert, K., Bayer, E., Guiochon, G.: Determination of the apparent transverse and axial dispersion coefficients in a chromatographic column by pulsed field gradient nuclear magnetic resonance. J. Chromatogr. A **694**, 321–331 (1995)

Baur, J., Kristensen, E., Wightman, R.: Radial dispersion from commercial high-performance liquid chromatography columns investigated with microvoltammetric electrodes. Anal. Chem. **60**, 2334–2338 (1988)

Brandt, A., Mann, G., Arlt, W.: Enhancement of the separation efficiency through temperature control in preparative high-performance liquid chromatography columns. J. Chromatogr. A 223–228 (1998)

Chaouki, J., Larachi, F., Dudokovic, M.: Non-invasive monitoring of multiphase flows. Ind. Eng. Chem. Res. **36**, 4476–4503 (1997)

Farkas, T., Chambers, J., Guiochon, G.: Column efficiency and radial homogeneity in liquid chromatography. J. Chromatogr. A **679**, 231–245 (1994)

Farkas, T., Sepaniak, M., Guiochon, G.: Column radial homogeneity in high performance liquid chromatography. J. Chromatogr. A **740**, 169–181 (1996)

Farkas, T., Guiochon, G.: Contribution of the radial distribution of the flow velocity to band broadening in HPLC columns. Anal. Chem. **69**, 4592–4600 (1997)

Farkas, T., Sepaniak, M., Guiochon, G.: Radial distribtion of the flow velocity, efficiency and concentration in a wide HPLC column. AIChE J. **43**, 1964–1974 (1997)

Götz, J., Zick, K., Heinen, C., König, T.: Visualisation of flow processes in packed beds with NMR imaging: determination of the local porosity, velocity vector and local dispersion coefficients. Chem. Eng. Pro. **41**, 611–629 (2002)

Guiochon, G., Lin, B.: In: Modeling for Preparative Chromatography, pp. 83–126. Academic Press, San Diego (2003)

Guiochon, G., Farkas, T., Guan-Sajonz, H., Koh, J.-H., Sarker, M., Stanley, B., Yun, T.: Consolidation of particle beds and packing of chromatographic columns. J. Chromatogr. A **762**, 83–88 (1997)

Harding, S., Baumann, H.: Nuclear magnetic resonance studies of solvent flow through chromatographic columns: effect of packing density on flow patterns. J. Chromatogr. A **905**, 19–34 (2001)

Heuer, C., Hugo, P., Mann, G., Seidel-Morgenstern, A.: Scale up in preparative chromatography. J. Chromatogr. A **752**, 19–29 (1996)

Kalender, W.: Computed Tomography, 2nd edn. Wiley, New York (2005)

Kamiński, M.: Simple test for determination of the degree of distortion of the liquid-phase flow profile in columns for preparative liquid chromatography. J. Chromatogr. **589**, 61–70 (1992)

Kantzas, A.: Computation of holdups in fluidized and trickle beds by computer-assisted tomography. AIChE J. **40**, 1254–1261 (1994)

Karacan, C.: An effective method for resolving spatial distribution of adsorption kinetics in heterogeneous porous media: application for carbon dioxide sequestration in coal. Chem. Eng. Sci. **58**, 4681–4693 (2003)

Knox, J.: Practical aspects of LC theory. J. Chromatogr. Sci. **15**, 352–364 (1977)

Lode, F., Rosenfeld, A., Yuan, Q., Root, T., Lightfoot, E.: Refining the scale-up of chromatographic separations. J. Chromatogr. **796**, 3–14 (1998)

McCullough, E., Payne, J.: X-ray-transmission computed tomography. Med. Phys. **4**, 85–98 (1977)

Mitchell, N., Hagel, L., Fernandez, E.: In situ analysis of protein chromatography and column efficiency using magnetic resonance imaging. J. Chromatogr. A **779**, 73–89 (1997)

Michel, M., Epping, A., Jupke, A.: Modeling and determination of model parameters. In: Schmidt-Traub, H. (ed.) Preparative Chromatography of Fine Chemicals and Pharmaceutical Agents. Wiley-VCH, Weinheim (2005)

Mogensen, K., Stenby, E., Zhou, D.: Studies of waterflooding in low-permeable chalk by use of X-ray CT scanning. J. Pet. Sci. Eng. **32**, 1–10 (2001)

Östergren, K., Trägårdh, C.: Characterization of hydrodynamic dispersion in a chromatographic column under compression. Chem. Eng. J. **79**, 103–111 (2000)

Peters, E., Hardham, W.: Visualization of fluid displacements in porous media using computed tomography imaging. J. Pet. Sci. Eng. **4**, 155–168 (1990)

Peters, E., Gharbi, R., Afzal, N.: A look at dispersion in porous media through computed tomography imaging. J. Pet. Sci. Eng. **15**, 23–31 (1996)

Schembre, J., Kovscek, A.: A technique for measuring two-phase relative permeability in porous media via X-ray CT measurements. J. Pet. Sci. Eng. **39**, 159–174 (1996)

Schulte, M., Epping, A.: Fundamentals and general terminology. In: Schmidt-Traub, H. (ed.) Preparative Chromatography of Fine Chemicals and Pharmaceutical Agents. Wiley-VCH, Weinheim (2005)

Sedermann, A., Johns, M., Bramley, A., Alexander, P., Gladden, F.: Magnetic resonance imaging of liquid flow and pore structure within packed beds. Chem. Eng. Sci. **52**, 2239–2250 (1997)

Sedermann, A., Johns, M., Alexander, P., Gladden, F.: Structure-flow correlations in packed beds. Chem. Eng. Sci. **53**, 2117–2128 (1998)

Seidel-Morgenstern, A.: Modeling of the competitive isotherms and the chromatographic separation of two enantiomers. Chem. Eng. Sci. **48**, 2787–2797 (1993)

Tallarek, U., Baumeister, E., Albert, K., Bayer, E., Guiochon, G.: NMR imaging of the chromatographic process migration and separation of bands of gadolinium chelates. J. Chromatogr. A **696**, 1–18 (1995)

Tallarek, U., Albert, K., Bayer, E., Guiochon, G.: Measurement of transverse and axial apparent dispersion coefficients in packed beds. AIChE J. **42**, 3041–3054 (1996)

Tallarek, U., van Dusschoten, D., Van As, H., Bayer, E., Guiochon, G.: Study of transport phenomena in chromatographic columns by pulsed field gradient NMR. J. Phys. Chem. B **102**, 3496–3497 (1998a)

Tallarek, U., Bayer, E., Guiochon, G.: Study of dispersion in packed chromatographic columns by pulsed field gradient nuclear magnetic resonance. J. Am. Chem. Soc. **120**, 1494–1505 (1998b)

Van Deemter, J., Zuiderweg, F., Klinkenberg, A.: Longitudinal diffusion and resistance to mass transfer as causes of nonideality in chromatography. Chem. Eng. Sci. **5**, 271–289 (1956)

Yun, T., Guiochon, G.: Modeling of radial heterogeneity in chromatographic columns. Columns with cylindrical symmetry and ideal model. J. Chromatogr. A **672**, 1–10 (1994)

Yun, T., Guiochon, G.: Modeling of radial heterogeneity in chromatographic columns. II. Separation of a two-component mixture on a column with cylindrical symmetry. J. Chromatogr. A **734**, 97–103 (1996)

Yun, T., Guiochon, G.: Visualization of the heterogeneity of column beds. J. Chromatogr. A **760**, 17–24 (1997)